Journal of Catalysis **204,** 292–304 (2001)
doi:10.1006/jcat.2001.3399, available online at http://www.idealibrary.com on IDEAL®

Influence of Pretreatment Temperature on the Bimetallic Interactions in Pt-Re/Al_2O_3 Reforming Catalysts Studied by X-Ray Absorption Spectroscopy

Magnus Rønning,* Torbjørn Gjervan,* Rune Prestvik,† David G. Nicholson,‡ and Anders Holmen*,[1]

*Department of Chemical Engineering, Norwegian University of Science and Technology (NTNU), N-7491 Trondheim, Norway; †SINTEF Applied Chemistry, N-7465 Trondheim, Norway; and ‡Department of Chemistry, Norwegian University of Science and Technology (NTNU), N-7491 Trondheim, Norway

Received February 16, 2001; revised August 3, 2001; accepted August 10, 2001

The influence of pretreatment temperature on the metal function of a commercial Pt-Re/Al_2O_3 reforming catalyst was studied by X-ray absorption spectroscopy. By simultaneously examining the rhenium L_{III} and platinum L_{III} EXAFS data, the bimetallic interaction and the metal-support interaction can be distinguished from the overall spectrum. The results show that if the catalyst is dried in air at temperatures $\leq$500°C before reduction at 480°C, bimetallic particles of platinum and rhenium are formed. Drying at higher temperatures and in absence of air inhibits the transport of mobile (rhenium) species on the surface causing no intimate contact between the two metals. Platinum L_{III} EXAFS data show that the average particle size of the bimetallic particles on the alumina surface is less than 10 Å. The results from the rhenium L_{III} EXAFS analysis confirm that rhenium is not completely reduced to metallic rhenium after reduction, with a significant fraction of the rhenium present in low, positive oxidation states and in intimate contact with the support. The EXAFS data are consistent with a structural model of rhenium metal particles 1–3 nm wide with smaller platinum particles situated within or at the boundary of the rhenium particles, and that moderate heating in presence of air (i.e., moist) provides the best conditions for transport of mobile rhenium species on the surface, and hence alloy formation.

Key Words: **catalyst pretreatment; platinum catalysts; rhenium; catalytic reforming; EXAFS; bimetallic interaction.**

INTRODUCTION

The catalytic reforming of naphtha is usually performed using a bifunctional catalyst containing both a hydrogenating metal and an acid function. The metal function is platinum together with another component such as rhenium, tin, iridium, or germanium. Chlorine-promoted alumina with high surface area provides the acid function. It has been demonstrated that the addition of rhenium to Pt/Al_2O_3 leads to a catalyst with greater stability and improved selectivity (1). However, the structure and exact role of rhenium in platinum-rhenium catalysts have been a matter of controversy. It has been proposed that metallic rhenium provides sites for hydrogenolysis of coke deposits (2) and that rhenium acts independently of platinum and is able to convert coke precursors into harmless products (3). Others state that rhenium anchors platinum to the alumina support and thereby stabilises the platinum dispersion (4). The structure-insensitive conversion of methylcyclohexane (MCH) has been used as a measure of the platinum dispersion in the catalysts.

The most common explanation of the properties of the catalyst is based on Pt–Re alloy formation (5) and the interaction of such an alloy with sulphur (6–9). It has been shown that the hydrogenolysis activity over bimetallic catalysts is significantly higher than over its monometallic counterparts (5, 10, 11) and also higher than for physical mixtures of Pt/Al_2O_3 and Re/Al_2O_3 (12). Hydrogenolysis is a structure-sensitive reaction and has therefore been used as a probe reaction to determine Pt–Re alloy formation. In addition, TPR-studies (13–15) have indicated possible reduction mechanisms leading to the formation of bimetallic Pt–Re metal particles. Previous studies indicate that the treatment of the catalyst prior to reduction strongly modifies the reducibility of rhenium and the extent of Pt–Re alloy formation (16–19). Varying degrees of alloy formation have been confirmed by both hydrogenolysis activity measurements and hydrogen chemisorption experiments (17). More direct evidence of alloy formation from physical characterisation techniques such as IR and XPS has been difficult to obtain due to the low metal loading and high metal dispersion in the Pt–Re reforming catalysts.

Studies using EDX and TEM (20, 21) conclude that no rhenium can be detected in the platinum particles in the bimetallic system after reduction at 400°C, although the yields from reforming experiments indicate that a significant fraction of the rhenium must be present in the metallic

[1] To whom correspondence should be addressed. Fax: +47 73 59 50 47. E-mail: holmen@chembio.ntnu.no.

0021-9517/01 $35.00

state. However, in a recent study (18) a high-resolution combined STEM and EDX instrument were able to detect bimetallic Pt–Re particles. It was established that bimetallic interaction in Pt–Re/Al_2O_3 catalysts is highly dependent on the pretreatment conditions. The highest degree of Pt–Re interaction was found when the catalyst was not dehydrated prior to reduction, while drying in N_2 at high temperatures before reduction causes sintering of platinum particles and low bimetallic interaction.

X-ray absorption spectroscopy (XAS) is a powerful technique for obtaining detailed information about the metal containing species in highly dispersed systems lacking long-range order. Several XAS studies on Pt–Re/Al_2O_3 have been reported dealing with different aspects concerning the metal function of the catalyst system. Recent studies have made use of TPR and binding energies from the XAS spectra to establish the correlation between calcination temperatures and bimetallic interaction (22). It is reported that rhenium is completely reducible to metallic rhenium if the samples are calcined at low temperatures and that the reduction step involves a rhenium intermediate with oxidation state close to +I (23) leading to complete alloying of platinum and rhenium. Michel *et al.* (24) found that the metal loadings and the Re/Pt ratio affect the reduction kinetics of rhenium but do not affect the final oxidation state of rhenium, and that even if the catalyst precursor is dried, all of the rhenium is coreduced with platinum at low temperatures when the catalyst contains ca. 1 wt% chlorine.

Fung *et al.* (25) used EXAFS to characterise Pt–Re clusters supported on γ-Al_2O_3 prepared from [$Re_2Pt(CO)_{12}$], demonstrating that by using k^0 weighting (k being the wave vector) contributions from metal-support interactions and bimetallic interaction (Pt–Re) may be distinguished in the EXAFS data analysis. They conclude that the catalyst reduced at 400°C in H_2 contained a considerable fraction of bimetallic particles consisting of Re_4Pt_2 entities and displaying high dispersion (average particle size less than 10 Å) and strong interaction between rhenium atoms and the support. For further details, we refer to Xiao and Puddephatt (26), who have published a comprehensive review on the structure and reactivity of Pt–Re clusters.

There are several experimental obstacles associated with XAS data collection on this catalyst system, with the most important being low metal loading. Samples with metal loadings as low as 0.3 wt% require the spectra to be recorded in the fluorescence mode rather than the transmission mode. Furthermore, interference from overlapping EXAFS regions excludes part of the EXAFS region associated with the platinum L_{III} and L_{II} absorption edges (27). Accordingly, one can either choose to use the limited EXAFS region associated with the platinum L_{III} and L_{II} edge or use the EXAFS associated with the platinum L_I edge, which is not affected by intervening rhenium edges but exhibits a considerably weaker signal compared to the L_{III} edge. By comparing preliminary data for all three platinum L edges, data associated with the platinum L_{III} adsorption edge (11,565 eV) were found to be most suitable for this EXAFS study. Due to the similarity in backscattering properties for the two noble metals involved, simultaneous investigations of data taken from representative reference systems and the use of both k^0 and k^3 weighting schemes are important for the deconvolution of contributions from the different backscatterers (25). We report here an examination of samples from four different pretreatment procedures by the use of X-ray absorption spectroscopy.

EXPERIMENTAL

Catalyst Pretreatment Procedure

The standard EUROPT-4 commercial catalyst (CK433) containing 0.3 wt% platinum and 0.3 wt% rhenium supported on γ-Al_2O_3 was manufactured by Akzo, Holland. The chlorine loading was 0.95 wt%. The precalcined EUROPT-4 catalyst extrudates were finely grounded and sieved to give a particle size fraction of 0.25–0.075 mm.

In order to use the allocated beam time at the ESRF and Brookhaven laboratories as efficiently as possible the samples were dried and reduced ex situ in our home laboratory. After reduction, the samples were sealed in quartz capillary tubes as described below to prevent exposure to air. This procedure avoids time-consuming in situ pretreatment at the synchrotron facility. In order to verify that the sealing procedure was successful, some of the samples were reduced in situ using an environmental cell developed by Lytle *et al.* (28).

Pretreatment was carried out in a standard apparatus equipped with Alltech molsieves and O_2-traps for gas purification. Steady gas flows (30 ml/min) were maintained by using mass-flow controllers. The catalyst was placed on a quartz sinter inside a tubular flow-through quartz microreactor with quartz capillary tubes (from Glas Technik & Konstruktion, Germany) with outer diameter 2–3 mm and wall thickness of 0.02 mm attached to the reactor wall. The sample was heated to the desired temperatures using a furnace equipped with a temperature controller. Four different drying conditions prior to reduction at 480°C for 1 h using a heating rate of 0.8°C/min were examined. One sample labelled PR-0 was reduced directly without any drying. A second sample labelled PR-240/air was dried in air at 240°C for 16 h before reduction. Another sample labelled PR-500/air was dried in air at 500°C for 16 h before reduction. The sample labelled PR-680/N_2 was dried in dry N_2 at 680°C for 16 h before reduction. After the reduction was finished the reactor was flushed with helium for 30 min and cooled down to room temperature. The reactor was sealed off at both ends using stainless steel valves and turned upside down to allow the powdered sample to enter

TABLE 1

Previously Obtained Data for the Catalyst Samples Involved (16, 17)

Sample Pt–Re/γ-Al_2O_3 (CK433)	Metal loading	Drying conditions	H/Pt ratio[a]	MCH Conversion[b]
PR-0	0.3/0.3 wt%	No drying	0.23	—
PR-240/air	0.3/0.3 wt%	240°C/air	0.31	41%
PR-500/air	0.3/0.3 wt%	500°C/air	0.44	42%
PR-680/N_2	0.3/0.3 wt%	680°C/N_2	0.16	27%

Note. All samples were reduced at 480°C in H_2 for 1 h after the indicated drying sequence (16 h).

[a] Volumetric hydrogen chemisorption at 25°C.

[b] Methylcyclohexane (MCH) conversion at 300°C, 1.1 bar, WHSV = 25 h^{-1}, and H_2/MCH = 40.

the capillary tubes. Using a relatively narrow sieve fraction of the catalyst powder (0.25–0.075 mm), easy filling and uniform distribution of the sample inside the capillary tube are ensured. The quartz tube containing the sample was sealed using a high-temperature gas flame, and detached from the reactor. The inert atmosphere inside the reactor and the relatively high flame temperature (>1200°C due to the high melting point for quartz) prevented oxidation of the catalyst PR-500/air inside the capillary tube. In order to reduce heat transfer to the sample in the capillary, the length of sample material was such that 2–3 cm of empty capillary separated the sample from the flame. A summary of the samples involved and their characteristics are given in Table 1. The volumetric hydrogen chemisorption measurements were performed in a Micromeretics ASAP 2010 instrument at 25°C.

XAS Measurements

XAS data were collected using the facilities of the Swiss-Norwegian Beamline (SNBL) at the European Synchrotron Radiation Facility (ESRF), France and at Beamline Station X11-A at the National Synchrotron Light Source (NSLS), Brookhaven National Laboratory. All spectra were collected at room temperature.

At SNBL, spectra were obtained on station EH1 at the platinum L_{III} edge (11,564 eV) and the rhenium L_{III} edge (10,535 eV). A channel-cut Si(111) monochromator with an unfocussed beam was used to scan the X-ray spectra. The beam currents ranged from 130 to 200 mA at 6.0 GeV. Higher order harmonics were rejected by means of a chromium-coated mirror angled at 3.5 mrad to give a cut-off energy of approximately 14 keV. The maximum resolution ($\Delta E/E$) of the Si(111) bandpass is 1.4×10^{-4} using a beam of size 0.6 × 7.2 mm as defined by the slits in the station. Ion chamber detectors with their gases at ambient temperature and pressure were used for measuring the intensities of the incident (I_0), transmitted (I_t), and fluorescent (I_f) X rays. The detector gases were as follows: I_0, detector length 17 cm, 100% N_2; I_t, length 31 cm, 35% Ar, 65% N_2; I_f (Lytle detector, see below), 100% Ar.

XAS data were also collected at Beamline Station X11-A at Brookhaven National Synchrotron Light Source. The station is equipped with a double crystal Si(111) monochromator and the storage ring is operated at 2.5 GeV with a ring current of 180–350 mA. The beam size was defined to be 0.5 × 10 mm and the resolution approximately 2.0×10^{-4} at the actual energies. Higher order harmonics were suppressed by tuning the monochromator crystals to 50% of maximum intensity.

The fluorescent radiation was collected using a detector of the type developed by Lytle *et al.* (28). The signal-to-noise ratio was enhanced using a set of soller slits and Zn (3μ) and Ga (3μ) filters for rhenium and platinum edges, respectively. Due to the low metal loading, several scans were taken and summed for each sample. The energy calibration was checked by measuring the spectrum of a platinum foil (thickness 0.003 mm) and a rhenium foil (thickness 0.0125 mm) with the energy of the first inflection point being defined as the edge energy. The raw, unfiltered Re L_{III} and Pt L_{III} EXAFS spectra of the four samples are shown in Fig. 1.

EXAFS Data Analysis

The data were corrected for dark currents, converted to k-space, and summed and the background was subtracted to yield the EXAFS function $\chi(k)$ using the EXCALIB and EXBACK programs (29). Model fitting was carried out with EXCURV90 using curved-wave theory and ab initio phase shifts (29, 30). During the least squares fitting it is important to minimise correlation effects between the parameters that strongly affect the EXAFS amplitude and those that influence the frequency of the EXAFS oscillations. Therefore, the EXAFS spectra were least squares fitted in k space using k^0 and k^3 weighted data. By carrying out this procedure on appropriate reference compounds as well as for the unknown spectra, more accurate coordination numbers can be obtained than what otherwise would be the case. The errors in the refined parameters (31–33) are estimated to be 10% in coordination number (N), 1% in distance (R), 10% in Debye–Waller type factors ($2\sigma^2$), and 10% in the photoelectron energy at zero wave vector (E_0). As an indication on the quality of the fit, the residual index, R_χ(%) is defined as

$$\chi = \frac{\sum_i \left[\left(\chi_i^{\exp} - \chi_i^{\text{calc}}\right)k^{WT}\right]^2}{\sum_i \left[\left(\chi_i^{\exp}\right)k^{WT}\right]^2} \times 100\%.$$

The k^3 weighting scheme compensates for the diminishing photoelectron wave at higher k values. Low k weighting also enhances the contribution from lighter backscattering atoms such as oxygen, and thereby allowing metal-support

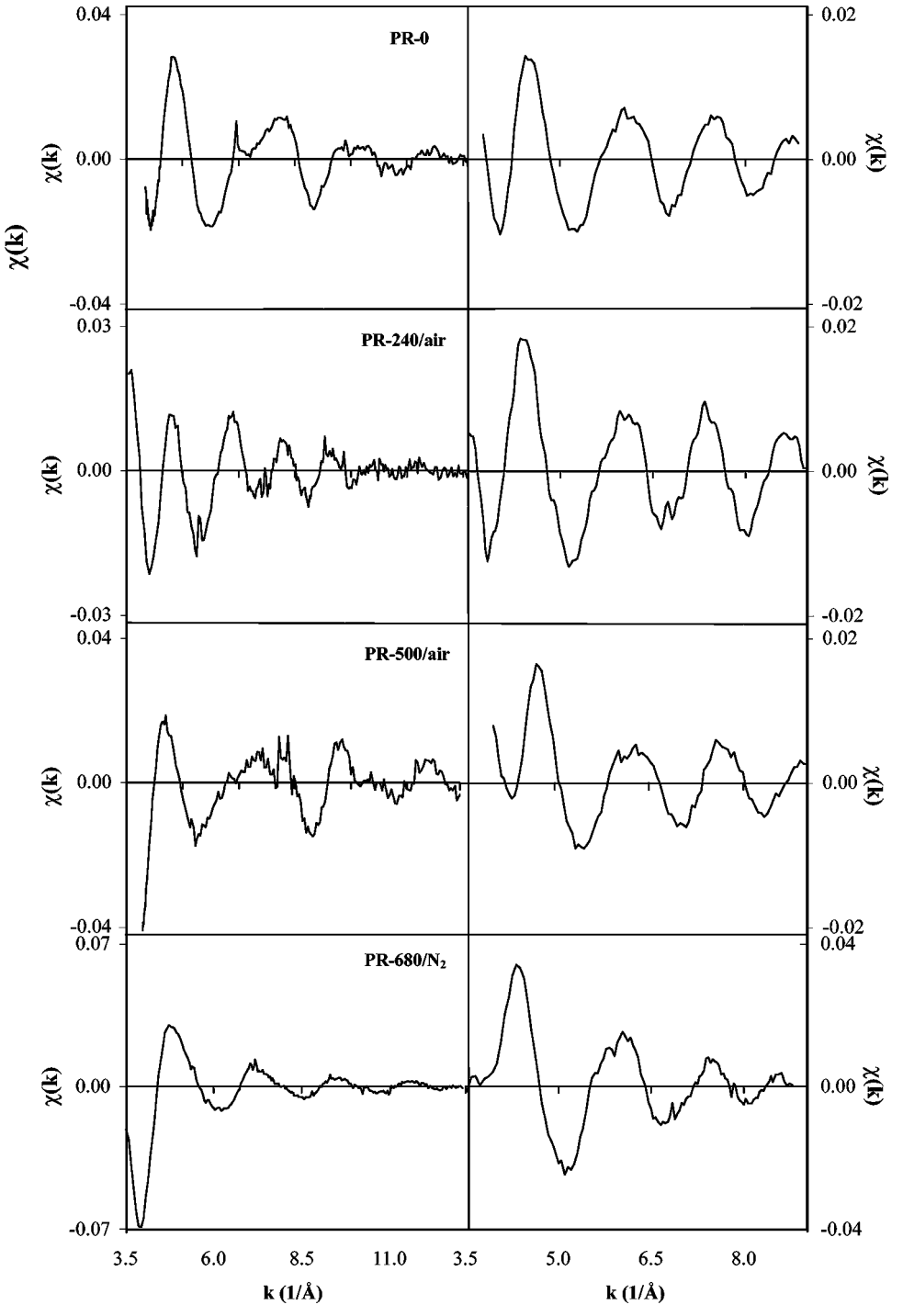

FIG. 1. The raw, unfiltered EXAFS spectra of the four samples from both the Re L_{III} edge (left) and the Pt L_{III} edge (right).

interactions to be included in the analysis. However, due to overlapping EXAFS regions for the platinum L_{III} and rhenium L_{II} edges, platinum L_{III} spectra have to be truncated at approximately 9 $Å^{-1}$. Our approach to the data analysis was similar to that used by Fung *et al*. (25). They demonstrated that by analysing the XAFS data using k^0 weighting, it is possible to distinguish Pt–Re from the Pt–Pt and Re–Re interactions. The parameters obtained by Fung *et al*. have been used as first guesses for the bimetallic interactions due to the lack of suitable model compounds for the Pt–Re and Re–Pt scattering pairs. The preliminary data analysis involved testing models that include contributions from Pt, Re, and O scatterers for both platinum and rhenium EXAFS data. Due to the narrow data range ($3.5\ Å^{-1} < k < 9.0\ Å^{-1}$) for the platinum L_{III} data, the distance (R) and disorder ($2\sigma^2$) for the Pt–Re coordination

TABLE 2

Crystallographic Data for the EXAFS Model Compounds Used to Check the Validity of the ab Initio Phaseshifts and Backscattering Amplitudes

Compound	Model pair	R (Å)[a]	N[b]	Reference
Re foil	Re–Re	2.74	12	(35)
$(NH_4)ReO_4$	Re–O	1.74	4	(37)
ReO_3	Re–O	1.87	6	(36)
Pt foil	Pt–Pt	2.77	12	(35)
PtO_2	Pt–O	2.00[c]	2 + 4	(38)

[a] Interatomic distance.
[b] Coordination number (multiplicity).
[c] Mean coordination distance, 2×1.989 Å$+ 4 \times 2.003$ Å $\cong$ 2.00 Å.

were kept fixed at the values obtained from the rhenium data analysis. This will keep the number of floating parameters (n) within the definition of the Nyquist criterion (34)

$$n = \left(\frac{2\Delta k \Delta r}{\pi}\right) + 1.$$

Rhenium L_{III} EXAFS data were fitted in the range $\Delta k = 3.5 - 13$ Å^{-1} using a Fourier filtering window ΔR, of 1.0 − 3.5 Å. Platinum L_{III} EXAFS data were fitted in the range $\Delta k = 3.5 - 9$ Å^{-1} and a Fourier filtering window ΔR, of 1.3 − 3.4 Å (1.0 − 3.4 Å for PR-680/N_2). In addition to the platinum and rhenium metal foils, ReO_3, $(NH_4)ReO_4$ (both the solid salt and an aqueous solution containing ReO_4^-) and PtO_2 were used as model compounds to check the validity of the ab initio phase shifts and establish the general parameters AFAC (amplitude reduction factor) and VPI (accounts for inelastic scattering of the photoelectron) (29). Structural parameters for the reference compounds (35–38) are listed in Table 2. The unreduced catalyst samples were used to check the validity of the amplitudes obtained from reference compounds measured in transmission mode for use on data of the reduced catalyst samples recorded in fluorescence mode.

XANES Profile Analysis

The XAS data analysis program WinXAS (39) was used for examining the XANES spectra of the reduced samples. The method of using a linear combination of the near-edge profiles from known reference compounds was used to obtain information about the composition of the samples of different pretreatment procedures. In order to establish the degree of reduction in the reduced samples, the edge profiles were analysed by linear combination of the reference profiles from the respective metal foil and the catalyst sample prior to reduction.

RESULTS AND DISCUSSION

EXAFS Analysis

The results from the rhenium L_{III} and platinum L_{III} EXAFS analysis are listed in Tables 3 and 4, respectively. The k^0 fitted rhenium L_{III} EXAFS spectra of the samples

TABLE 3

Results from the EXAFS Analysis of Data from the Re L_{III} Edge after Pretreatment and Reduction at 480°C

Sample	Drying conditions	Coord. shell	E_0 (eV)[a]	Quality of fit[b] (%)	N[c]	$2\sigma^2$ (Å^2)[d]	R (Å)[e]
PR-0	No drying	Re–Pt	20.4(2)	22.89	2.0(2)	0.033(3)	2.75(2)
		Re–Re			4.1(2)	0.025(1)	2.56(1)
		Re–O			1.5(1)	0.003(0)	1.72(1)
		Re–$O_{support}$			1.3(1)	0.004(0)	2.02(1)
PR-240/air	240°C/air	Re–Pt	18.2(2)	20.66	4.8(2)	0.033(2)	2.75(1)
		Re–Re			5.2(2)	0.023(1)	2.59(1)
		Re–O			0.4(1)	0.003(1)	1.93(1)
		Re–$O_{support}$			1.1(1)	0.006(1)	2.13(1)
PR-500/air	500°C/air	Re–Pt	12.2(5)	31.81	5.2(4)	0.030(2)	2.75(1)
		Re–Re			3.3(3)	0.014(1)	2.55(1)
		Re–O			1.5(1)	0.004(0)	1.76(1)
		Re–$O_{support}$			2.4(1)	0.006(0)	2.05(1)
PR-680/N_2	680°C/N_2	Re–Pt	9.5(1)	12.10	0	—	—
		Re–Re			1.5(1)	0.024(2)	2.74(1)
		Re–O			2.0(1)	0.004(0)	1.74(0)
		Re–$O_{support}$			0.9(1)	0.004(1)	1.96(0)

[a] Energy threshold.
[b] Defined in the text.
[c] Number of neighbours (multiplicity).
[d] Debye–Waller type factor (disorder).
[e] Interatomic distance.

TABLE 4

Results from the EXAFS Analysis of Data from the Pt L_{III} Edge after Pretreatment and Reduction at 480°C

Sample	Drying conditions	Coord. shell	E_0 (eV)[a]	Quality of fit[b] (%)	N[c]	$2\sigma^2$ (Å^2)[d]	R (Å)[e]
PR-0	No drying	Pt–Re	14.8(3)	17.64	1.1(2)	0.033([e])	2.75([f])
		Pt–Pt			2.9(1)	0.005(1)	2.66(4)
		Pt–$O_{support}$			0.2(1)	0.012(4)	2.69(7)
PR-240/air	240°C/air	Pt–Re	10.5(3)	10.30	1.1(2)	0.033([e])	2.75([f])
		Pt–Pt			2.5(1)	0.004(1)	2.67(2)
		Pt–$O_{support}$			0.5(0)	0.005(4)	2.70(8)
PR-500/air	500°C/ air	Pt–Re	24.7(5)	18.91	1.3(3)	0.030([e])	2.75([f])
		Pt–Pt			2.9(1)	0.006(1)	2.67(4)
		Pt–$O_{support}$			0	—	—
PR-680/N_2	680°C/ N_2	Pt–Re	14.1(1)	9.63	0	—	—
		Pt–Pt			3.6(1)	0.007(1)	2.67(3)
		Pt–$O_{support}$			0.8(1)	0.005(3)	2.63(6)
		Pt–O[g]			1.4(1)	0.006(1)	1.97(1)

[a] Energy threshold.
[b] Defined in the text.
[c] Number of neighbours (multiplicity).
[d] Debye–Waller type factor (disorder).
[e] Interatomic distance.
[f] Disorder ($2\sigma^2$) and distance (R) are kept fixed at values obtained from the Re L_{III} EXAFS analysis (see Table 3).
[g] Pt–O coordination associated with passivated/unreduced Pt.

together with their Fourier transforms are shown in Fig. 2, and the platinum L_{III} spectra of the same samples are presented in Fig. 3. For the rhenium EXAFS, a structural model including four shells, Re–Pt, Re–Re, and two different Re–O distances associated with Re(+VII) oxide species and support interaction, respectively, gave the best fit and realistic structural parameters for all samples except PR-680/N_2, which did not contain the contribution from the Re–Pt shell. The platinum spectra of PR-0, PR-240/air, and PR-500/air were best fitted using a model constructed from Pt–Re, Pt–Pt, and one single Pt–O contribution, the latter originating from metal-support interaction. The EXAFS spectrum of PR-680/N_2, which was consistently lacking the bimetallic interaction, was modelled by one Pt–Pt distance and two different Pt–O contributions.

The relatively large Re–Re and Re–Pt coordination numbers show that the rhenium containing metal particles of the samples in this study are significantly larger than the rhenium containing particles in the similar catalysts studied by Fung *et al.* (25). This is also reflected in the EXAFS spectra in Fig. 2, where the oscillations persist as far out as $k = 13$ Å^{-1}. The oscillations may also be affected by the extent of alloy formation in the metal particles since the Re–Re and the Re–Pt signals are out of phase within the region 10–13 Å^{-1}(25). The total metal-to-metal coordination is six to nine atoms for all of the samples except PR-680/N_2, which is coordinated to only 1.5 metal atoms. A relatively high proportion of the rhenium atoms in PR-680/N_2 is not completely reduced, and therefore exhibits relatively high coordination to oxygen and thus correspondingly lower metallic coordination. The rhenium EXAFS spectra of PR-0 and PR500/air contain more features than the spectra of PR-240/air and PR-680/N_2, indicating enhanced composite natures for the former. The spectrum from PR-680/N_2 is simplified due to the fact that there is only one metal–metal contribution. The complexity in the spectra from samples PR-0 and PR-500/air may arise from contributions from oxides with rhenium in different oxidation states. For example, ReO_3 has a collinear arrangement of O–Re–O atoms and hence multiple scattering processes contributing to the spectrum. However, this contribution is not large enough to be extracted from the overall spectrum, which is reflected in the relatively poor quality of the fit for PR-500/air (see Table 2). The slightly longer Re–O distance (1.76 Å) in PR-500/air compared to ReO_4^- (1.74 Å) is consistent with this since the Re–O distance in ReO_3 is 1.87 Å. In PR-240/air, the Re–O distance is even longer (1.93 Å), being close to the Re–O distance found in PR-680/N_2 at 1.96 Å. This Re–O distance is most likely associated with rhenium atoms in low oxidation states coordinated to oxygen in the support interface. The low coordination number (0.4) of the oxygen shell at 1.93 Å in PR-240/air coupled with the partially overlapping support interaction found at 2.13 Å indicate that the reliability of this distance is limited. The coordination shell is, however, included in the fitting since the contribution is statistically significant at the 1% level (40).

From the rhenium EXAFS analysis, PR-240/air and PR-500/air have the highest degrees of alloy formation (highest Re–Pt coordination). PR-0, which is not dehydrated prior to reduction, shows a significantly lower bimetallic coordination than PR-240/air and PR-0 and PR-500/air. This does not agree with previous reports (13, 41) suggesting that

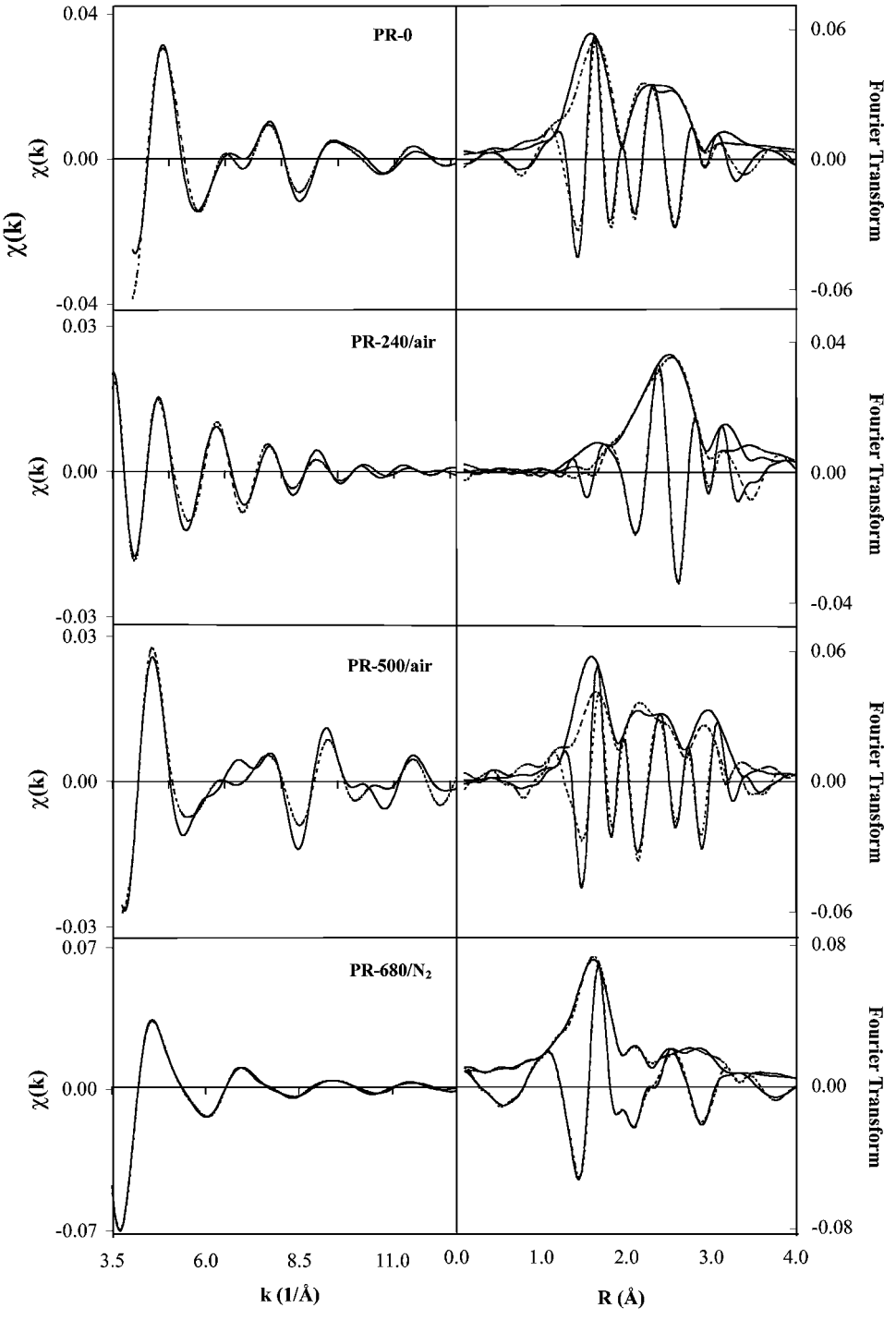

FIG. 2. Re L_{III} EXAFS spectra (left) and corresponding Fourier transforms (right) of all samples, using $\Delta k = 3.5 - 13$ Å^{-1} and $\Delta R = 1.0 - 3.5$ Å. Experiment is shown in solid lines and k^0 fit in dotted lines.

rhenium is more easily reduced when water is present on the surface allowing mobile rhenium oxide species to transport rhenium to the platinum particles. This discrepancy may be due to the fact that a significant fraction of the rhenium atoms is not completely reduced and that rhenium in low oxidation states may affect the mobility of rhenium atoms (23). The EXAFS data from PR-240/air exhibits the most balanced coordination towards platinum and rhenium (4.8 and 5.2, respectively). PR-240/air also contains a larger fraction of completely reduced rhenium. Consequently, moderate heating in air (i.e., low drying temperature) prior to reduction provides the most suitable conditions for transport

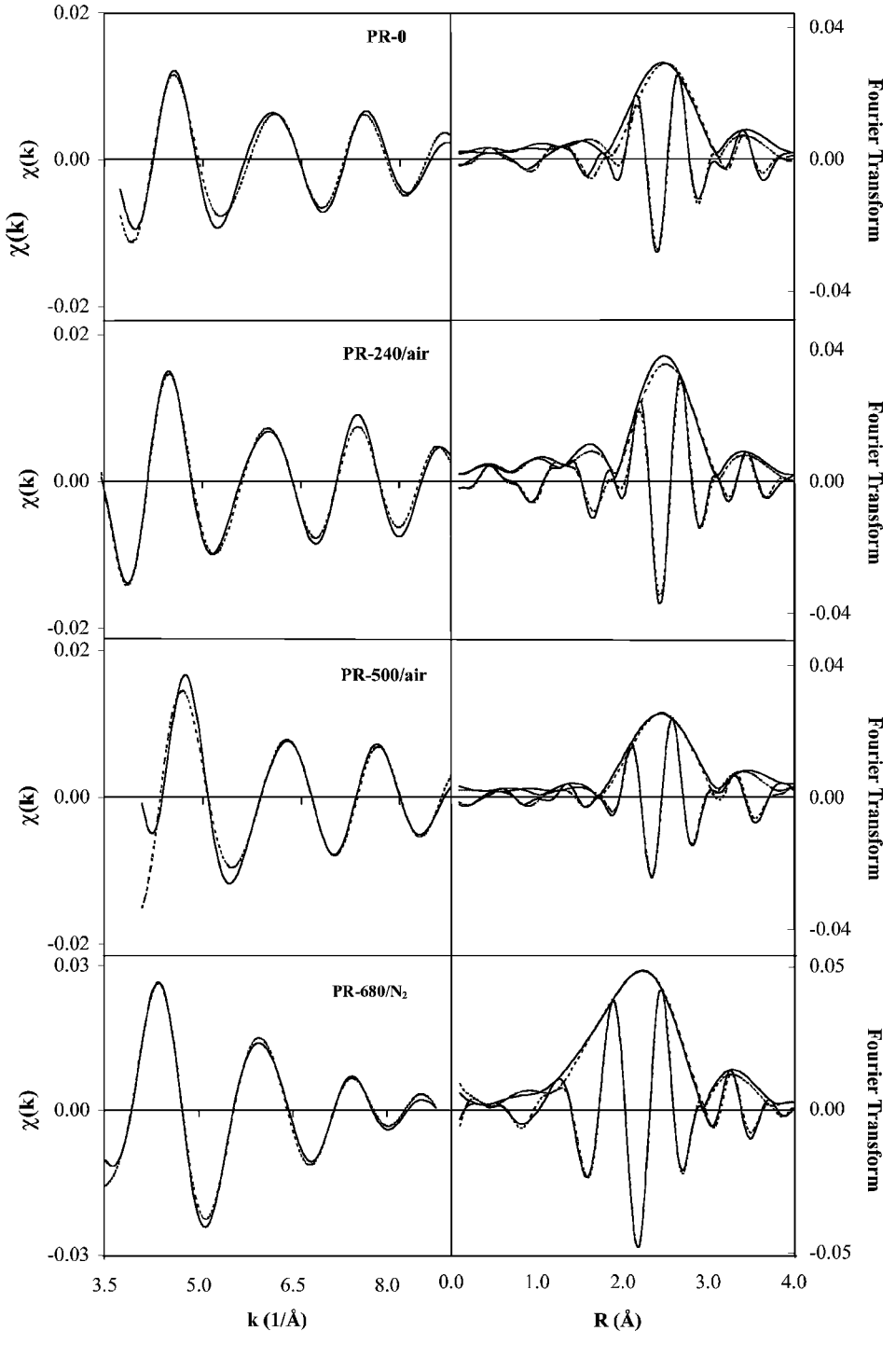

FIG. 3. Pt L_{III} EXAFS spectra (left) and corresponding Fourier transforms (right) of all samples, using $\Delta k = 3.5 - 9.0$ Å^{-1} and $\Delta R = 1.3 - 3.4$ Å. Experiment is shown in solid lines and k^0 fit in dotted lines.

of the mobile rhenium species on the surface, and hence alloy formation. For the sample dried in N_2 at high temperature (PR-680/N_2), the EXAFS analysis for both elements is consistent with this model and also with our previous EDX results (18) confirming that very limited alloying takes place under such conditions. The relatively low alloy formation in PR-0 is not reflected in the EXAFS analysis of the other element, platinum, which accords well with the aforementioned EDX results (see Tables 4 and 5). The results from the platinum EXAFS analysis show only minor differences between samples PR-0, PR-240/air, and PR-500/air. All three samples are characterised by a Pt–Pt

TABLE 5

Comparison of Average Platinum Atomic Fractions, C_{Pt}, in the Metal Particles and Particle Size Estimates for the Catalyst Samples from STEM/EDX Analysis (18) and EXAFS Analysis

	Pt fraction, C_{Pt}			Average particle diameter (nm)		
Sample	EDX	Pt EXAFS	Re EXAFS	STEM	Pt EXAFS[a]	Re EXAFS[a]
PR-0	0.65	0.72	0.33	0.9	<1.0	1.1
PR-240/air	0.68	0.69	0.48	1.0	<1.0	2.5
PR-500/air	0.81	0.69	0.61	1.8	<1.0	2.1
PR-680/N_2	0.92	1.00	0.00	2.3	<1.0[b]	<1.0[b]

[a] Mean particle diameter estimated from EXAFS data as described by Borgna *et al.* (50).
[b] Partially reoxidised.

coordination of ca. 3 and Pt–Re coordination close to 1. The relatively weak metal-support interaction at ca. 2.7 Å found in PR-0 and PR-240/air is not significant for PR-500/air. It has been reported that this metal-oxygen distance is typical for support interfaces, where chemisorbed hydrogen is present and when reduced at temperatures less than 450°C (25, 42, 43). It thus appears that raising the drying temperatures has an impact on the platinum-support interface similar to that when the reduction temperatures are raised, when dried in air (i.e., in presence of moisture), since PR-680/N_2 has a similar Pt–O distance, although slightly contracted. PR-680/N_2 displays a different spectrum from the other samples in the sense that, as stated above, it contains no bimetallic contribution and a somewhat stronger interaction with the support than the other samples. The strength of the interaction is reflected both in the higher Pt–O coordination and in the contracted metal-support bonding distance compared to the metal-support interaction in the other samples (see Table 4). Another difference is that PR-680/N_2 is not completely reduced, or more likely passivated (reoxidised) by oxygen after reduction. The Pt–Pt coordination is practically the same in this sample as for the three other samples. Thus, the larger particle sizes found in the STEM images of this sample (18) are not reflected in the EXAFS results. Since STEM is not able to distinguish between platinum metal and the oxide, this would indicate that the outermost atomic layers of larger platinum particles are easily passivated (44, 45) leading to smaller metal particles and hence reduced coordination numbers.

The structural parameters obtained from the rhenium and platinum EXAFS analysis can be summarised as follows: rhenium metal shows relatively high coordination to both rhenium and platinum in addition to a strong metal-support interaction, suggesting that relatively large (up to 3 nm) rhenium particles are present on the surface. Platinum EXAFS analysis shows high platinum dispersion (small particles consisting of only a few atoms) coordinated to both platinum and rhenium. These observations are consistent with a metal particle model in which rhenium particles are sited on the support interface. Smaller platinum particles are situated within or at the boundary of the rhenium particles. This is only true for the samples PR-0, PR-240/air, and PR-500/air, which contain bimetallic particles. The EXAFS analysis of PR-680/N_2 confirms that the surface contains separate particles of rhenium and platinum metal.

Particle Size and Composition

The high surface relaxations observed in small metal particles may lead to a significant contraction of the metal–metal bond distances relative to the distances found for bulk metal and to anharmonic pair distribution functions (46–48). For small metal particles, the average, nearest neighbour bond length decreases rapidly with decreasing particle diameter. Furthermore, the pair distribution functions become increasingly anharmonic for smaller particle sizes and may lead to significant errors in the estimation of coordination number and hence particle sizes. Consequently, particle size estimates from EXAFS are usually associated with relatively large uncertainty (ca. 20%). However, from the low Pt-metal coordination (ca. 4) in the investigated samples we conclude that the mean particle diameter in the platinum containing samples must be small. The contraction in Pt–Pt distances from 2.77 Å found for bulk platinum down to approximately 2.67 Å in the catalyst samples are also an indication of small particles. Klimenkov *et al.* (47) showed in a TEM study that a Pt–Pt atomic distance of 2.65 Å corresponds to a mean particle size of ca. 15 Å while Diaz-Moreno *et al.* used EXAFS to determine that first shell Pt–Pt coordination of 4 corresponded to a particle size of approximately 8 Å (48). It has been suggested that Pt–Pt coordination of 4.8 atoms corresponded to particles of diameter ca. 9 Å and containing about 10 atoms (49, 50). It may therefore be concluded that all samples contain platinum metal particles of average diameter less than 10 Å and that the platinum dispersion is 100%.

The Re–Re distances are even more contracted compared to bulk rhenium (2.74 Å). Samples PR-0, PR-240/air,

and PR-500/air have Re–Re bond lengths of ca. 2.6 Å even though the metal–metal coordination number is larger than for platinum. Such shortened Re–Re distances have been explained by presence of oxophilic rhenium in a low positive oxidation state (25). The atomic fractions of platinum C_{Pt}, listed in Table 5 are calculated by dividing the Pt–Pt coordination number by the total Pt-metal coordination number. The results from the platinum EXAFS analysis show negligible difference in C_{Pt} for samples PR-0, PR-240/air, and PR-500/air, whereas PR-680/N_2 shows no alloy formation. These results are practically identical with the EDX results, although a weak trend towards higher Pt–Re interaction for the samples dried at the lowest temperature could be observed (18). The EXAFS results show that C_{Pt} values obtained from the Re data are significantly different than the values from the Pt edge data. This inconsistency indicates that the samples also contain monometallic particles. This is in contrast to the STEM/EDX studies, which assume that all of the rhenium atoms are located in the bimetallic particles such that $C_{Re} = 1 - C_{Pt}$. Note that PR-240/air, which shows the highest hydrogenolysis activity of the four samples (18), has got the highest bimetallic interaction ($C_{Pt} = 0.48$).

Linear Combination of XANES Spectra

The shape of the absorption edge features and the white line intensity contain information about the oxidation state and chemical environment of the element in question. The graphical presentation in Fig. 4 of the rhenium L_{III} absorption edge profiles clearly shows that rhenium is not completely reduced. The XANES profile analysis gives a measure of the fraction of completely reduced rhenium in the sample. The amount of metallic rhenium deduced from the EXAFS data is based on the reduction in Re–O coordination number. From Table 6 it appears that EXAFS overestimates the degree of reduction (relative to the total amount of reducible rhenium). The number from the EXAFS analysis excludes that fraction of irreducible (under these conditions) rhenium that is in intimate contact with the support. By including the metal-support coordination number in the Re–O coordination number, the results from the EXAFS and XANES data converge to agreement. PR-240/air has a larger fraction of metallic rhenium than the other samples, suggesting that the higher reducibility of rhenium leads to a higher degree of alloying, thus supporting the previously proposed rhenium reduction mechanism (15, 18).

The XANES analysis of platinum L_{III} edge data is consistent with the EXAFS data of the same element, showing that practically all platinum is present as metallic platinum in the samples PR-0, PR-240/air, and PR-500/air, while

TABLE 6

Fraction of Metallic Re and Metallic Pt Determined from Linear Combination of XANES Profiles by Using the Metal Foil and the Unreduced PR-0s Reference Compounds

	Fraction of reduced Re		Fraction of reduced Pt	
Sample	XANES[a]	EXAFS[a]	XANES	EXAFS
PR-0	0.44	0.63	0.97	1.00
PR-240/air	0.45	0.90	0.98	1.00
PR-500/air	0.11	0.63	1.00	1.00
PR-680/N_2	0.04	0.50	1.00	0.77

Note. Numbers are obtained from EXAFS data by dividing the Re–O coordination number by the Re–O coordination number of the unreduced sample ($N = 4$) and by dividing the Pt–O coordination number by the Pt–O coordination number for the unreduced sample ($N = 6$).

[a] For sample PR-0 reduced in situ: XANES; 0.54, EXAFS; 0.78.

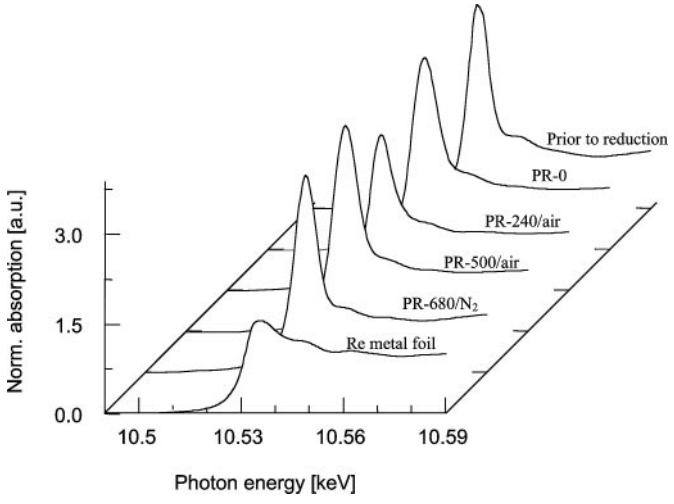

FIG. 4. Normalised Re L_{III} edge profiles and white line intensities for the catalyst samples shown together with the profiles of a rhenium foil and the unreduced sample (CK433) as references.

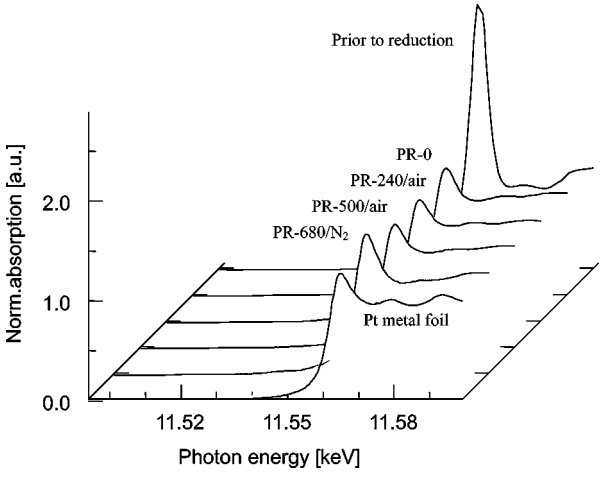

FIG. 5. Normalised Pt L_{III} edge profiles and white line intensities for the catalyst samples shown together with the profiles of a platinum foil and the unreduced sample (CK433) as references.

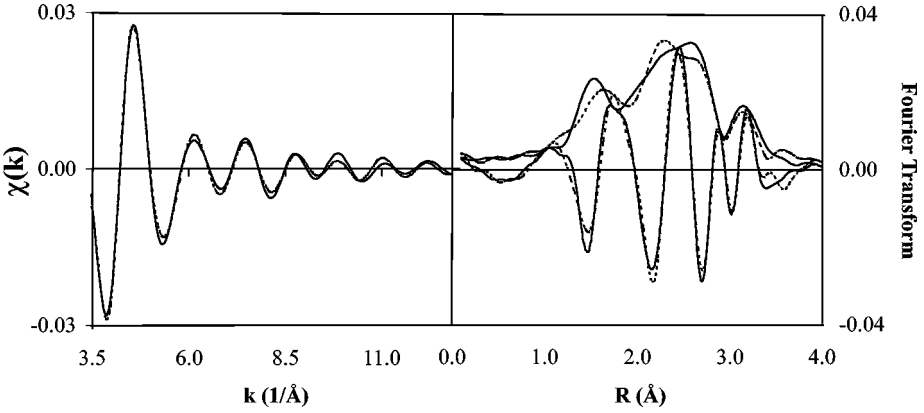

FIG. 6. Re L_{III} EXAFS spectrum (left) and corresponding Fourier transform (right) of the sample PR-240/air reduced *in situ*, using $\Delta k = 3.5 - 13$ Å^{-1} and $\Delta R = 1.0 - 3.5$ Å. Experiment is shown in solid lines and k^0 fit in dotted lines.

PR-680/N_2 is slightly reoxidised (see Table 6). This is also reflected in the white line intensities of the platinum catalyst samples shown in Fig. 5, which are all very similar to the profile of the platinum metal foil.

Passivation

PR-0 was reduced *in situ* (in the X-ray beam) as a test in order to establish whether or not the sample was reoxidised in the quartz capillary tubes. The fitted EXAFS spectrum of the sample is shown in Fig. 6. The EXAFS data in Table 7 show that the amount of completely reduced rhenium is higher in the *in situ* reduced sample with the fraction of Re(0) being 78% compared to 63% in the sample sealed in a capillary tube. No significant reoxidation of platinum was found. The reoxidation can be considered as passivation of the metal particles since it is limited to the surface layers. Passivation by oxygen of supported platinum particles has been reported as being mainly limited to the surface layer and hence proportional to the fraction of surface platinum atoms (44, 50, 51). The oxide layer has Pt–O distances close to that of PtO_2 (ca. 2.00 Å), which is the most stable platinum oxide. Surface chloride complexes may also be involved in the oxidation of the metal particles when chloride is present in the system (52, 53). The Re–Re coordination number is practically the same for the samples sealed in capillary tubes and the one reduced *in situ*, while the Re–Pt coordination is considerably lower and the Re–O coordination accordingly higher in the passivated sample (see Fig. 7). These results may explain why Macleod *et al.* (21) in their TEM/EDX study were unable to detect any neither bimetallic interaction nor metallic rhenium in their catalyst samples. Most of the rhenium may have been oxidised to higher oxidation states since the bimetallic particles seem to be more prone to reoxidation than the particles containing only rhenium. The weakened bimetallic interaction in the quartz capillary sample compared to the in situ reduced sample also indicate that the true bimetallic contributions in the Pt–Re catalyst are larger than what are reported here.

TABLE 7

Comparison of the Re L_{III} EXAFS Data from the Sample PR-240/Air Reduced *in Situ* and the Same Sample Reduced *ex Situ* (at Our Home Laboratory) and Subsequently Sealed in a Quartz Capillary Tube

	Reduced in situ		Reduced ex situ	
Backscattering pair	N^a	R (Å)^b	N^a	R (Å)^b
Re–Pt	5.2	2.75	2.0	2.75
Re–Re	3.8	2.63	4.1	2.56
Re–O	0.9	1.77	1.5	1.72
Re–$O_{support}$	1.5	2.04	1.3	2.02

[a] Coordination number (multiplicity).
[b] Interatomic distance.

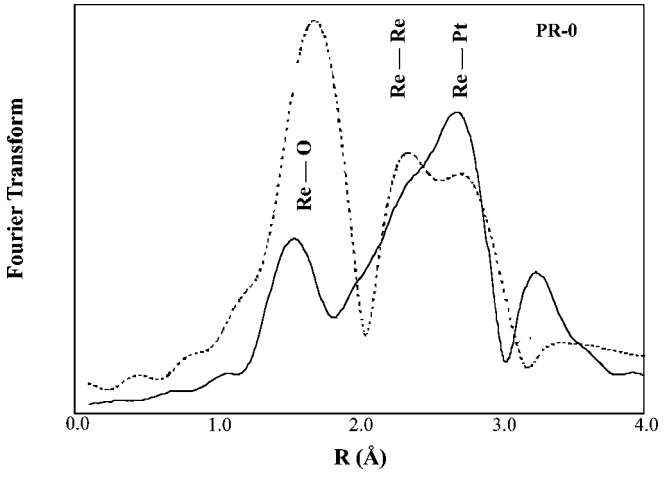

FIG. 7. Fourier transforms of the Re L_{III} EXAFS spectra of PR-240/air reduced *in situ* (solid line) and of the same sample reduced *ex situ* and sealed in a quartz capillary tube (dotted line).

CONCLUSIONS

The effect of the pretreatment conditions on the metal particles in Pt-Re/Al_2O_3 catalysts was studied for several pretreatment procedures, using X-ray absorption spectroscopy and by comparison with previous results obtained by STEM/EDX (18) and catalytic measurements (17).

The results show that if the catalysts are dried in air at temperatures $\leq$500°C before reduction at 480°C, bimetallic particles of platinum and rhenium are formed. Drying at higher temperatures in absence of air inhibits the transport of mobile (rhenium) species on the surface causing no intimate contact between the two metals. Platinum L_{III} EXAFS data show that the average particle size of the bimetallic particles on the alumina surface is less than 10 Å. The results from the rhenium L_{III} EXAFS analysis confirm that rhenium is not completely reduced to metallic rhenium in the catalysts after reduction. The short Re–Re distance (ca. 2.6 Å) suggests that oxophilic rhenium in low, positive oxidation states are present. Rhenium interacts relatively strongly with the support, which is reflected in the Re–O interaction around 2.0 Å that displays an average coordination number close to 1.0.

EXAFS data from the rhenium edge exhibits higher coordination numbers towards platinum and rhenium than those obtained from the platinum EXAFS data. The relatively high Re–Re and Re–Pt coordination, together with the strong Re-support interaction, and platinum being coordinated to approximately 1 rhenium and 3 platinum atoms, agree with a structural model of rhenium metal particles 1–3 nm wide with smaller platinum particles situated within or at the boundary of the rhenium particles.

The catalyst sample dried at 240°C in air prior to reduction at 480°C (PR-240/air) contains more completely reduced rhenium than the other samples. The EXAFS data from this sample exhibits the most balanced coordination towards platinum and rhenium. These results show that moderate heating in presence of air (i.e., moist) provides the best conditions for transport of mobile rhenium species on the surface, which is necessary for alloy formation.

ACKNOWLEDGMENTS

The authors thank the Research Council of Norway for the financial support of this work. We acknowledge the staff at the Swiss-Norwegian Beam Lines at ESRF for their assistance (Experiment Number 01-01-98), and we thank the Norwegian University of Science and Technology and the Research Council of Norway for grants towards construction and maintenance of SNBL. The Brookhaven National Synchrotron Light Source (Beamline X11A) is thanked for generously providing beamtime. The NSLS is supported by the U.S. Department of Energy under Contract Numbers DE-AC02-76CH00016 and DE-FG05-89ER45384. Support from the Nansen Foundation and VISTA-Statoil (both to DGN) is acknowledged. Scientific glassblower Tor Johannes Wærøe at SINTEF Applied Chemistry is acknowledged for his assistance in the work involving the quartz capillary tubes.

REFERENCES

1. Kluksdahl, H. E., U.S. Patent 3,415,737, 1968.
2. Parera, J. M., and Beltramini, J. N., *J. Catal.* **112**, 357 (1988).
3. Bertolacini, R. J., and Pellet, R. J., *in* "Catalyst Deactivation" (B. Delmon and G. F. Froment, Eds.), p. 73. Elsevier, Amsterdam, 1980.
4. Yermakov, Y. U., and Kuznetsov, B. N., *J. Mol. Catal.* **9**, 13 (1980).
5. Betizeau, C., Leclercq, G., Maurel, R., Bolivar, C., Charcosset, H., Frety, R., and Tournayan, L., *J. Catal.* **45**, 179 (1976).
6. Biloen, P., Helle, J. N., Verbeek, H., Dautzenberg, F. M., and Sachtler, W. M. H., *J. Catal.* **63**, 112 (1980).
7. Shum, V. K., Butt, J. B., and Sachtler, W. M. H., *J. Catal.* **96**, 371 (1985).
8. Ribeiro, F. H., Bonivardi, A. L., Kim, C., and Somorjai, G. A., *J. Catal.* **150**, 186 (1994).
9. Augustine, S. M., Alameddin, G. N., and Sachtler, W. M. H., *J. Catal.* **115**, 217 (1989).
10. Haining, I. H. B., Kemball, C., and Whan, D. A., *J. Chem. Res.* (S), 170 (1977).
11. Haining, I. H. B., Kemball, C., and Whan, D. A., *J. Chem. Res.* (S), 364 (1978).
12. Shum, V. K., Butt, J. B., and Sachtler, W. M. H., *J. Catal.* **99**, 126 (1986).
13. Wagstaff, N., and Prins, R., *J. Catal.* **59**, 434 (1979).
14. Isaacs, B. H., and Petersen, E. E., *J. Catal.* **77**, 43 (1982).
15. Augustine, S. M., and Sachtler, W. M. H., *J. Catal.* **116**, 184 (1989).
16. Prestvik, R., Ph.D. thesis, Norwegian Institute of Technology, Trondheim, 1995.
17. Prestvik, R., Grande, K., Moljord, K., and Holmen, A., *J. Catal.* **174**, 119 (1998).
18. Prestvik, R., Tøtdal, B., Lyman, C. E., and Holmen, A., *J. Catal.* **176**, 246 (1998).
19. Reitmaier, S. F., Subramaniam, A., and Sermon, P. A., *Catal. Lett.* **19**, 345 (1993).
20. Huang, Z., Fryer, J. R., Park, C., Stirling, D., and Webb, G., *J. Catal.* **148**, 478 (1994).
21. Macleod, N., Fryer, J. R., Stirling, D., and Webb, G., *Catal. Today* **46**, 37 (1998).
22. Hillbrig, F., Michel, C., and Haller, G. L., *J. Phys. Chem.* **96**, 9893 (1992).
23. Fernandez-Garcia, M., Chong, F. K., Anderson, J. A., Rochester, C. H., and Haller, G. L., *J. Catal.* **182**, 199 (1999).
24. Michel, C., Bambrick, W. E., Ebel, R. H., Larsen G., and Haller, G. L., *J. Catal.* **154**, 222 (1995).
25. Fung, A. S., Kelley, M. J., Koningsberger, D. C., and Gates, B. C., *J. Am. Chem. Soc.* **119**, 5877 (1997).
26. Xiao, J., and Puddephatt, R. J., *Coord. Chem. Rev.* **143**, 457 (1995).
27. Meizner, G., Via, G. H., Lytle, F. W., and Sinfelt, J. H., *J. Chem. Phys.* **87**(11), 6354 (1987).
28. Lytle, F. W., Greegor, R. B., Marques, E. C., Sandstrom, D. R., Via, G. H., and Sinfelt, J. H., *J. Catal.* **95**, 546 (1985); Lytle, F. W., Greegor, E. C., Sandstrom, R. B., Marques, D. R., Wong, J., Spiro, C. L., Huffman, G. P., and Huggins, F. D., *Nucl. Instr. Meth.* **226**, 542 (1984).
29. Binsted, N., Campbell, J. W., Gurman, S. J., and Stephenson, P. C., EXCALIB, EXBACK, and EXCURV90 programs, SERC Daresbury Laboratory, 1990.
30. Gurman, S. J., Binsted, N., and Ross. I., *J. Phys. C: Solid State Phys.* **17**, 143 (1984).
31. Koningsberger, D. C., and Prins, R., Eds., "X-ray Absorption: Principles, Applications, Techniques of EXAFS, SEXAFS and XANES." Wiley, New York, 1988.

32. Lytle, F. W., Sayers, D. E., and Stern, E. A., Eds., "Report of the International Workshop on Standards and Criteria in X-ray Absorption Spectroscopy." *Physica B* **158**, 701 (1989); Hasnain, S. S., Ed., "Report of the International Workshop on Standards and Criteria in X-ray Absorption Spectroscopy." X-ray Absorption Fine Structure. Ellis Horwood, Chicester, 1991.
33. Vaarkamp, M., *Catal. Today* **39**, 271 (1998).
34. Stern, E. A., *Phys. Rev. B* **48**, 9825 (1993).
35. MacGillavry, C. H., Riek, G. D., and Lonsdale, K., Eds., *in* "International Tables of X-ray Crystallography," Vol. III, p. 281. Kynock Press, Birmingham, UK 1962.
36. Meisel, K., *Z. Anorg. Allg. Chem.* **207**, 121 (1932).
37. Brown, R. J. C., Segel, S. L., and Dolling, G., *Acta Crystallogr.* **B36**, 2195 (1980).
38. Range, K.-J., Rau, F., Klement, U., and Heyns, A. M., *Mat. Res. Bull.* **22**, 1541 (1987).
39. Ressler, T., *J. Physique IV* **7**, C2 (1997).
40. Joyner, R. W., Martin, K. J., and Meehan, P., *J. Phys. C: Solid State Phys.* **20**, 4005 (1987).
41. Bolivar, C., Charcosset, H., Frety, R., Primet, M., Tournayan, L., Betizeau, C., Leclercq, G., and Maurel, R., *J. Catal.* **39**, 249 (1975).
42. van Zon, F. B. M., Maloney, S. D., Gates, B. C., and Koningsberger, D. C., *J. Am. Chem. Soc.* **115**, 10,317 (1993).
43. Vaarkamp, M., Modica, F. S., Miller, J. T., and Koningsberger, D. C., *J. Catal.* **144**, 611 (1993).
44. McCabe, R. W., Wong, C., and Woo, H. S., *J. Catal.* **114**, 354 (1988).
45. Shido, T., Lok, M., and Prins, R., *Topics Catal.* **8**, 223 (1999).
46. Clausen, B. S., Topsøe, H., Hansen, L. B., Stolze, P., and Nørskov, J. K., *J. Catal.* **114**, 463 (1994).
47. Klimenkov, M., Nepijko S., Kuhlenbeck, H., Bäumer, M., Schlögl, R., and Freund, H.-J., *Surf. Sci.* **391**, 27 (1997).
48. Diaz-Moreno, S., Koningsberger, D. C., and Munoz-Paez, A., *Nucl. Instr. Met. Phys. Res. B* **133**, 15 (1997).
49. Kip, B. J., Duivenvoorden, F. B. M., Koningsberger, D. C., and Prins, R., *J. Catal.* **105**, 26 (1987).
50. Borgna, A., Le Normand, F., Garetto, T., Apesteguia, C. R., and Moraweck, B., *Catal. Lett.* **13**, 175 (1992).
51. Markusse, A. P., Kuster, B. F. M., Koningsberger, D. C., and Marin, G. B., *Catal. Lett.* **55**, 141 (1998).
52. Le Normand, F., Borgna, A., Garetto, T., Apesteguia, C. R., and Moraweck, B., *J. Phys. Chem.* **100**, 9068 (1996).
53. Borgna, A., Garetto, T., Apesteguia, C. R., Le Normand, F., and Moraweck, B., *J. Catal.* **186**, 433 (1999).